Published in The European Physical Journal B - Condensed Matter and Complex Systems 18, issue 2, 215-225, 2000
which should be used for any reference to this work

Preparation and characterization of clean, single-crystalline YH_x films ($0 \leqslant x \leqslant 2.9$) on W(110)

J. Hayoz,[a] Th. Pillo, M. Bovet, and A. Züttel
Institut de Physique, Université de Fribourg, Pérolles, CH-1700 Fribourg, Switzerland

St. Guthrie
Surface Chemistry Department, Sandia National Laboratories, Livermore, California 94551-0969

G. Pastore
SAES Getters S.p.A., Viale Italia 77, 20020 Lainate, MI, Italy

L. Schlapbach and P. Aebi
Institut de physique, Université de Fribourg, Pérolles, CH-1700 Fribourg, Switzerland

Yttrium can be loaded with hydrogen up to high concentrations causing dramatic structural and electronic changes of the host lattice. We report on the preparation of clean, single-crystalline YH_x films ($0 \leqslant x \leqslant 2.9$). The films have been characterized *in situ* combining angle-resolved photoelectron spectroscopy (ARPES) and low energy electron diffraction. Direct Y dihydride growth, i.e., Y evaporation under a H_2 partial pressures of $\approx 5 \times 10^{-6}$ mbar at 500 K on W(110), is the most convenient starting point for the preparation of clean single-crystalline Y hydride films covering H concentrations from the ''clean metal'' ($x \approx 0$) up to the lower boundary of the pure trihydride phase ($x \approx 2.9$). Upon annealing Y dihydride films the desired H concentration can be adjusted within the α-phase or the ($\alpha+\beta$) two-phase regime. On the other hand, the extension of our photoelectron spectrometer with an homemade ultrahigh vacuum (UHV) compatible hydrogenation system allows to induce the transition from Y dihydride to Y trihydride within a few minutes. The hydrogenation system combines a high-pressure reaction cell with hydrogen permeation through a Pd–24%Ag tube. The overall design is such that the sample never gets in contact with non-UHV compartments. For direct Y dihydride growth on W(110) two equally populated face-centered-cubic(111) domains rotated by 180° with respect to each other are observed. In the α- and γ-phase the Y atoms form a hexagonal-close-packed(0001) oriented lattice. Furthermore, the previously established model for *in situ* H concentration estimation in Y [J. Hayoz *et al.*, Phys. Rev. B **58**, R4270 (1998)] is extended successfully from the α to β to the β to γ-phase transition. Ultraviolet photoemission spectroscopy data unequivocally reveal the opening of a gap extending as far as 1 eV below E_F for normal electron emission upon the phase-transformation from Y dihydride to Y trihydride. It also appears that the H absorption rate strongly depends on the H_2 purity. Our experimental results demonstrate the capability of this setup for *in situ* preparation and investigations on the geometrical and electronic structure of Y hydride films and, more generally, rare-earth hydride films using ARPES.

I. INTRODUCTION

The interaction of hydrogen with Y, La, and the rare-earth (RE) metals has been the subject of numerous investigations due to the interesting temperature- and concentration-dependent structures and properties observed in the solid solution (α-phase) as well as in the dihydride (β) and trihydride (γ) phases.[1] An example is the recent observation of switchable optical properties of Y and La hydride films where shiny, metallic dihydride films become transparent semiconductors in the trihydride phase.[2] It is obvious that the knowledge of the geometrical and electronic structure of RE hydrides is the key for the understanding of all these properties.

For Y, the crystal structure of the host lattice and the hydrogen atom positions are well known over the entire range of H concentrations ($x = \mathrm{H/Y}$): Y crystallizes in the hexagonal-close-packed (hcp) structure, while its dihydride occurs in a face-centered-cubic (fcc) CaF_2-type structure.[1] The trihydride, finally, possesses a hcp unit cell (HoD_3 type).[3] The electronic structure of Y hydrides, however, is still a matter of dispute.[1] In particular the electronic nature of the optically transparent state in yttrium is presently not well understood, and has, therefore, stimulated the interest of theoreticians.[4–9]

One reason why the nature of the ground state of Y hydrides has not been firmly established and the mechanism of the hydrogen-induced metal–insulator transition has eluded clarification is that to date no experimental, *k*-resolved band-structure data are available in the literature.[1] Properly speaking angle-resolved ultraviolet photoemisson (ARUPS) is *the* method for that purpose. However, two main problems hin-

[a]Present address: Department of Physics, The Pennsylvania State University, University Park, PA 16802; electronic mail: joh4@psu.edu

dered the successful outcome of ARUPS experiments: On the one hand, loss of single crystallinity is difficult to avoid during the first transition (α to β) and most bulk samples decompose into powder while going from β to γ.[1] Obviously, this does not comply with one fundamental condition of ARUPS experiments, namely the single crystallinity of the sample under investigation. On the other hand, oxygen contamination is a serious problem for photoemission experiments on Y hydrides. Indeed, all existing photoemission spectroscopy data from polycrystalline bulk samples reported the O contamination level to be in the order of 5%–15% (cross section corrected O $1s$/Y $3d$ ratios).[10–13] Experiments probing the valence band structure, i.e., using photon energies lower than ≈100 eV, are particularly sensitive because of the unfavorably high p/d cross-section ratio. Consequently, the measured valence-band structure becomes falsified by slightest surface contaminations.

Thin polycrystalline Y films evaporated under very good ultrahigh vacuum (UHV) conditions were reported to be much cleaner than bulk samples.[14] Moreover, epitaxially grown Y films are promising to improve the structural stability during H loading and unloading. Indeed, a recent x-ray diffraction study demonstrated, that in thin, single-crystalline Y films grown on Nb(110) the structural coherence is maintained during cycling *ex situ* between the dihydride and the trihydride phases.[15] In contrast to previous studies using bulk sensitive methods,[2,3,15–17] for photoemission studies of Y as a function of the hydrogen content the films cannot be capped with a protective Pd layer and, therefore, H loading and unloading must be done *in situ*. Moreover, in order to avoid any surface contamination, the hydrogen gas used to load the films must be as clean as possible.

Recently we reported on the reversibility of hydrogen loading in thin single-crystalline Y films grown by vapor deposition on W(110) without loss of single crystallinity.[18] It was demonstrated that under a H_2 partial pressure of 1×10^{-5} mbar (700 K during 2 h) clean, hcp(0001) oriented Y films convert to fcc(111) oriented Y dihydride films. However, due to the residual gas the O contamination level of Y and Y dihydride films was found to increase by ≈0.2% per hour (cross section corrected O $1s$/Y $3d$ ratios) even at very good UHV conditions and, consequently, our Y dihydride films were contaminated by ≈0.4% O. Thus, once the Y deposition is accomplished, a procedure to prepare the different hydride phases within a few minutes is necessary for reliable photoemission experiments.

In a conventional UHV surface analysis system H loading is limited to low plateau pressure hydride phases such as the Y dihydride phase. Indeed, the equilibrium pressure at the isothermal of Y dihydride is very low (10^{-6} mbar at 800 K), whereas at room temperature (RT) hydrogen pressures above 1×10^{-3} mbar are required to induce the transition from β to γ.[1] Moreover, the time needed to transform the complete Y film into the trihydride phase is governed by the external hydrogen pressure. In the case of *ex situ* loading of Pd capped Y films the transition takes about one hour at 10 mbar, whereas it typically takes 15 min at 250 mbar.[19] We therefore expect that upon exposure to H_2 pressures in the range of 1 bar clean, uncapped Y films completely transform to the trihydride phase within a few minutes. Thus, for reliable photoemission experiments H loading up to the pure trihydride phase must be done within an UHV compatible high-pressure reaction cell (HPRC).

In this study we demonstrate that it is possible to prepare clean, single-crystalline YH_x films ($0\leqslant x\leqslant 2.9$) on W(110) and to vary their H concentration without loss of order. In contrast to previous studies,[2,15–17] preparation and characterization are done *in situ*, and the films are not capped by a protective Pd layer. It will be shown that direct Y dihydride growth, i.e., Y evaporation under a H_2 partial pressures of $\approx5\times10^{-6}$ mbar at 500 K on W(110), is the most convenient starting point for the preparation of clean Y hydride films covering H concentrations from the ''clean metal''[20] ($x\approx0$) up to the lower boundary of the pure γ-phase ($x\approx2.9$). We would like to point out that it is the development of our homemade UHV compatible hydrogenation system presented in Sec. III, that made it possible to prepare clean, single-crystalline Y hydride films within the β-phase the ($\beta+\gamma$) two-phase regime, and the pure γ-phase. We used x-ray photoelectron diffraction (XPD) and low-energy electron diffraction (LEED) to observe the near surface changes occurring due to the H-induced structural transitions. Based on XPD and hydrogen-induced core-level shifts we propose a model for an *in situ* estimate of the H concentration in Y. Furthermore, we present first ARUPS data of Y as a function of the H content. However, in the context of the present paper we will emphasize on preparation procedure, i.e., study the effect of contamination on the measured spectra as well as the influence of the H_2 purity on the H adsorption rate. The H-induced metal–insulator transition in Y, which is unequivocally confirmed by the ARUPS spectra, will be discussed elsewhere.[21]

The article is organized as follows. The particular experimental setup and procedures are described in Sec. II. Section III presents the design and operation of the homemade, UHV compatible hydrogenation system. In Sec. IV we discuss our experimental results. Finally, we summarize our findings in Sec. V.

II. EXPERIMENTAL PROCEDURES

We used XPD to observe, in real space and near the surface, the changes occurring due to the H-induced structural transitions in yttrium. XPD has been chosen because of its chemical sensitivity and its sensitivity to local real-space order. It is a powerful technique for surface structural investigations,[22] and it has been shown that full hemispherical XPD patterns provide very direct information about the near-surface structure.[18,23–27] At photoelectron kinetic energies above about 500 eV, the strongly anisotropic scattering by the ion cores leads to a forward focusing of the electron flux along the emitter-scatterer axis. The photoelectron angular distribution, therefore, is to a first approximation a forward-projected image of the atomic structure around the photoemitters. LEED, in contrast, shows the symmetry of

reciprocal space, is not chemically selective, and contains information about the long-range order of the atoms near the surface.

The XPD data are presented in so-called diffractograms, i.e., in a stereographic projection and in a linear gray scale image with maximum intensity corresponding to white (see Fig. 4). The center of each plot corresponds to the surface normal (polar emission angle $\Theta=0°$) while the outer circle represents directions parallel to the surface ($\Theta=90°$). Single-scattering cluster (SSC) calculations have been used to interpret the XPD patterns. The SSC model used for photoelectron diffraction is discussed in detail elsewhere.[22] Note, that the cross section for forward scattering increases with increasing atomic number.[28] Therefore, forward scattering due to H atoms is generally too weak to be observed. H atoms, consequently, have been neglected in all simulations.

The experiments were performed in a Vacuum Generators ESCALAB Mk II spectrometer modified for motorized sequential angle-scanning data acquisition,[23,24] equipped with a three-channeltron hemispherical electrostatic energy analyzer and with a base pressure in the low 10^{-11} mbar region. The core of the experimental setup is the custom made two-axis sample goniometer. The goniometer allows a computer-controlled rotation of the sample in polar and in azimuthal direction with an accuracy better than 0.5°. The range in polar direction is going from grazing electron emission along the crystal surface up to normal electron emission. On the analysis position, i.e., on the goniometer, the sample can be heated up to 1000 K and cooled down to about 120 K with LN_2. Photoclectron spectra and diffraction patterns were measured using Mg $K\alpha$ ($h\nu=1253.4$ eV) radiation. Mapping electronic states over the Brillouin zone within reciprocal space is realized using a monochromatized multiple energy laboratory ultraviolet source.[29] This so-called *k*-space mapping results in dispersion plots and cuts through constant energy surfaces, e.g., the Fermi surface (FS).[24,30,31] Furthermore, using a VG AG 60-185 ion gun for low energy ion scattering spectroscopy, it is possible to do angle-scanned ion scattering for structural studies of the topmost layers.[32] The preparation chamber (base pressure 2×10^{-11} mbar) is equipped with a LEED setup, a Danish Micro Engineering[33] scanning tunneling microscope, and sample preparation facilities (a sputter gun, heating facilities, and LN_2 cooled evaporation sources). In the context of the present study the preparation chamber has been extended with our homemade UHV compatible hydrogenation system presented in Sec. III.

The substrate used to prepare the Y hydride films was a W(110) single crystal. In order to deplete C from the W(110) crystal, it was annealed to 1500 K for 125 h under an O_2 partial pressure of 10^{-7} mbar. Subsequently, the crystal was flashed to 2500 K.[34] As a result no C or O contaminations could be detected with x-ray photoelectron spectroscopy (XPS) and LEED displayed well-defined and sharp (1×1) spots indicating a well ordered surface. As revealed by LEED and FS mapping, RT growth of Y on W(110) without any H_2 background pressure ends up with a rough and disordered surface. Often, the surface quality can be improved by an increased mass transport at the surface, i.e., upon annealing and/or deposition at higher substrate temperatures. Indeed, for Y deposition above ≈850 K very sharp LEED patterns were observed. However, the overlayer appears to agglomerate (a kind of Ostwald ripening) into large three-dimensional (3D) crystals. This conclusion is based on the observation that for 200-Å-thick films (quartz oscillator reading) deposited above/below ≈850 K the W substrate could/could not be detected with XPS, respectively. For Y growth on W(110) without any H_2 background pressure best compromise between rough surfaces and 3D crystallite formation was found at ≈600 K.[18] Y deposition under an H_2 partial pressure of $\approx5\times10^{-6}$ mbar, in contrast, is well reproductible and yields well defined, clean single-crystalline Y dihydride films (see Sec. IV) for substrate temperatures ranging from RT up to 600 K. In analogy to the recent observation of hydrogen-promoted self-diffusion of Pt atoms on Pt(110) surfaces,[35] hydrogen-promoted self-diffusion of Y atoms on the hcp Y surface may account for this finding. If not otherwise specified, the Y films discussed in the present study therefore were prepared by depositing high purity Y (99.99%) from a LN_2 cooled electron-bombardment evaporation cell under a hydrogen partial pressure of 5×10^{-6} mbar with the W(110) crystal held at 500 K. During Y deposition the film thickness was controlled by means of a water-cooled quartz microbalance. All films discussed in the present article were 200 Å thick. After Y deposition the W $4f$ doublet was no longer detectable, i.e., the W(110) substrate was completely covered with Y, and, most importantly, *no O contamination* could be detected with XPS.

In order to vary the H concentration after deposition (see Sec. IV) the Y dihydride films either were annealed (H unloading), or were exposed up to 1000 mbar purified H_2 within the HPRC (H loading). LEED pictures at different energies were taken for each film. Thereafter the samples were transferred *in situ* to the two-axis goniometer in the analysis chamber. Care was taken that the H loading/unloading procedure, the LEED experiment, and the sample transfer to the analysis position were done within 15 min after the Y deposition was accomplished.

For each film we then measured He I exited valance band spectra. Subsequently, line shape and peak position of the Y $3d$ doublet as well as the O $1s$ core level were probed with XPS. Most satisfactory we note, that ≈30 min after Y deposition the oxygen contamination level still was below the limit of detectability of XPS. For each Y hydride film an Y $3d_{5/2}$ diffractogram [$E_{\mathrm{kin}}\approx1097$ eV (the exact kinetic energy of the Y $3d_{5/2}$ photoelectrons depends on the H concentration)] was measured. The data acquisition procedure for obtaining these diffractograms consists in measuring series of azimuthal (ϕ) scans, at polar angle intervals of $\Delta\theta=2°$. It begins at $\theta_{\mathrm{start}}=80°$ off normal and terminates at $\theta_{\mathrm{end}}=0°$. The azimuthal angular step size at any polar angle is chosen such that the solid-angle sampling density is uniform. Typical data acquisition times were 8 h at a pressure of 4×10^{-11} mbar. After all these experiments, i.e., ≈8.5 h after Y deposition, the O $1s$ signal is clearly detectable with XPS.

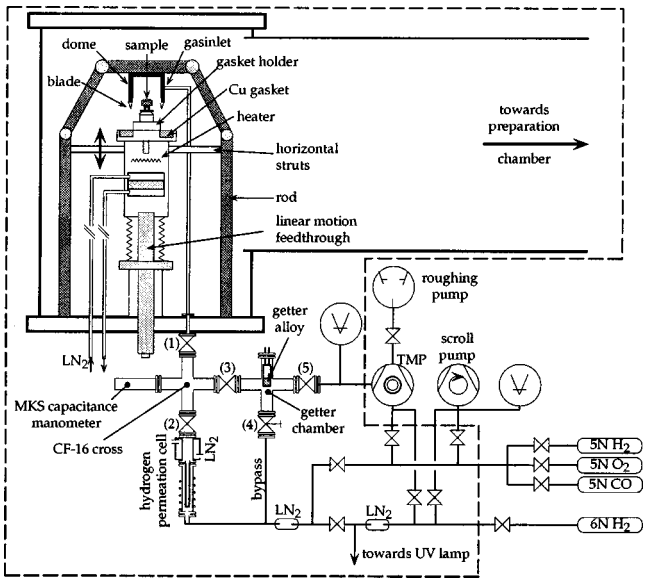

FIG. 1. Sketch of the UHV compatible hydrogenation system used for the *in situ* preparation of clean, single-crystalline Y hydride films within the β-phase, the $(\beta+\gamma)$ two-phase regime, and the γ-phase. Note, that it is not to scale. The HPRC is mounted on a CF-150 flange. The hatched line encloses the bakeout area.

We find that, independent of the H concentration, the O contamination level of the Y hydride films increased by $\approx$0.2% per hour (cross section corrected O 1*s* to Y 3*d* intensity ratio). Note that almost the same evolution of the O contamination level was reported by Baptist *et al.* for polycrystalline Y films grown and handled under similar UHV conditions.[14]

III. HYDROGENATION SYSTEM

Figure 1 shows the HPRC and the hydrogen permeation cell together with the chart of the relevant gaspipes and pumps. The hatched line encloses the bakeout area. All materials, if not otherwise specified, are stainless steel. We exclusively used all metal valves and CF fittings. Temperature was controlled by means of chromel-alumel thermocouples.

A. HPRC and getter chamber

The HPRC (mounted on a CF-150 flange and connected to the preparation chamber of the spectrometer) essentially consists of a dome with a sharp blade and a Cu gasketholder screwed on a linear motion feedthrough (see Fig. 1). Three massive rods, which root in the CF-150 flange, hold the dome in a fixed position. The Cu gasket is soldered into the holder. The sampleholder is transferred with a wobblestick on the pin in the center of the gasketholder. A thermocouple just located below the gasketholder allows for temperature control during heating or cooling with LN_2 (for clarity Fig. 1 does not show all details). By means of the linear motion feedthrough the gasketholder can be moved upwards until the sharp blade of the dome crushes into the Cu gasket. A torque of $\approx$30 Nm is required to tighten the HPRC against the main UHV vessel. A very accurate guidance of the Cu gasket with respect to the blade is crucial for its multiple use. This guidance is provided by three horizontal struts fixed on the linear motion feedthrough sliding on the three vertical rods as well as by the cylindrical landing in the center of the gasketholder positioning the blade. Nevertheless, the gasketholder can be exchanged *in situ* by means of the same wobblestick as used for the sample transfer.

Via the 6 mm gasinlet tube, one reaches a first CF-16 cross equipped with a bakeable MKS absolute capacitance manometer covering the 1.3×10^{-1}–$1.3\times10^{+3}$ mbar pressure range. By means of the CF-16 edge valves (1), (2), and (3) the first cross can be separated form the HPRC, the hydrogen permeation cell, and a second CF-16 cross in the following referred to as getter chamber, respectively. As can be seen from the chart the setup provides the use of different gases. However, only hydrogen can penctrate through the hydrogen permeation cell (see Sec. III B). All other gases must flow through the bypass pipe in order to be dosed with the CF-16 leak valve (4). Valve (5) finally, gives access to a turbomolecular pump (TMP) allowing for an independent ventilation of the gassystem. The nonoperational mode is with valves (1), (2), (3), and the HPRC open, whereas valves (4) and (5) are closed, i.e., the cross, the getter chamber as well as the downstream side of the hydrogen permeation cell are connected with the main UHV vessel via the gasinlet tube.

The getter chamber contains two pills ($\approx$2 g) of the SAES Getters[36] getter alloy ST707® (70%Zr–24.6%V–5.4%Fe) known to have a wide operating temperature range, including RT. A homemade pill holder enables temperature control of the getter alloy using a thermocouple as well as heating the pills up to 900 °C. Heating under UHV conditions is required to activate the getter. This process causes the passive oxide layer formed at the getter surface when handling in air to diffuse into the bulk. Optimal activation is reached when the getter is heated to 450 °C for 10 min.[36]

Once the getter is activated various gaseous impurities such as H_2, H_2O, CO, CO_2, and N_2 which contact the surface, are captured and chemisorbed onto the getter. For ST707®, operating temperatures above $\approx$200 °C insure a diffusion rate of the chemisorbed atoms into the bulk of the getter sufficient to avoid passivation layer formation, thus allowing utilization of the full getter capacity. Once sorbed, oxygen, carbon, and nitrogen atoms cannot be released again by the ST707® even at very high temperatures, due to the formation of strong chemical bonds with the alloy atoms. Hydrogen isotopes react differently, however. They diffuse into ST707® getter body more quickly than other atoms and distribute almost uniformly within the bulk even at low temperatures. In addition, because of the relatively weak forces that bind these atoms to the alloy, the hydrogen isotopes sorbed at low temperatures can be released at temperatures ranging from 500 to 900 °C, depending upon the application. Therefore, if the alloy is used as a hydrogen pump, its full getter capacity can always be restored upon heating. Moreover, the alloy can be used not only as a pump but also as a solid reservoir and a purifier for hydrogen isotopes.[37]

In our application the task of the getter alloy is twofold. First, it compensates for the bad pumping of the CF-16 cross,

the getter chamber, and the downstream side of the hydrogen permeation cell through the small gas inlet tube. Second, this oil-free pumping unit is used to evacuate the HPRC from hydrogen (see later).

B. Hydrogen permeation cell

It is well known that hydrogen (and its isotopes) permeates easily through palladium membranes via a solution-diffusion mechanism, i.e., dissociative chemisorption of H_2, dissolution and diffusion of atomic hydrogen through the membrane, and subsequent desorption of H_2. However due to hydrogen embrittlement, a phenomenon in which dissolved hydrogen initiates cracks at the boundaries between the solid solution and the hydride phase—eventually causing rupture on repeated pressure and temperature cycling—pure palladium membranes cannot be used below 300 °C.[38] This defect of palladium can be reduced by alloying with group 1b metals such as silver.[39] The reduced stress at the phase boundaries and, thus, the increased resistance to embrittlement is attributed to the higher hydrogen solubility in these alloys as compared to pure palladium.[40] The permeation rate of hydrogen through Pd–24%Ag alloys can primarily be increased by decreasing the membrane thickness. Indeed, tube-shaped specimens with very thin walls (≈0.1 mm) turned out to have a high hydrogen permeation rate as well as to endure stress caused by concentrational dilatations, typically of the order of 3%–4%, better than other geometries.[41]

The selective hydrogen permeability of Pd alloy membranes is widely used. Most importantly we note that filtering devices based on these alloys permit to remove all impurities from gaseous hydrogen as well as to separate high-quality hydrogen (or its isotopes) from gas mixtures with high selectivity (up to 10^{10}).[41] Other applications involve catalytic membrane reactors where continuous withdrawal of hydrogen from the reaction mixture avoids the equilibrium limitation of a reaction, e.g., the dehydrogenation of methanol or hydrocarbons, by the so-called drain-off effect.[42] Obviously, such devices can also be used as hydrogen generators. The possibility to separate the different hydrogen isotopes finally, is based on the different heats of solution and diffusion mobilities of protium, deuterium and tritium in Pd alloys.[41]

Figure 2(a) shows the detailed structure of our homemade hydrogen permeation cell which is based on a Pd–24%Ag tube. The advantage of this tube is that it has very thin walls (≈0.1 mm) and a large surface area (length ≈100 mm; outer diameter ≈6 mm) favorable for high permeation rates. The open end of the Pd–24%Ag tube was Ag soldered on a stainless steel tube which in turn is welded on the CF-16 flange of the downstream tube (outer diameter=10 mm). As can be seen from Fig. 2(a) the welding seam is within the blades of the CF-16 flange and therefore the interior of the Pd–24%Ag tube is part of the UHV environment. The operating temperature is measured using a thermocouple that is welded onto the surface of the upstream tube next to a constantan filament heater.

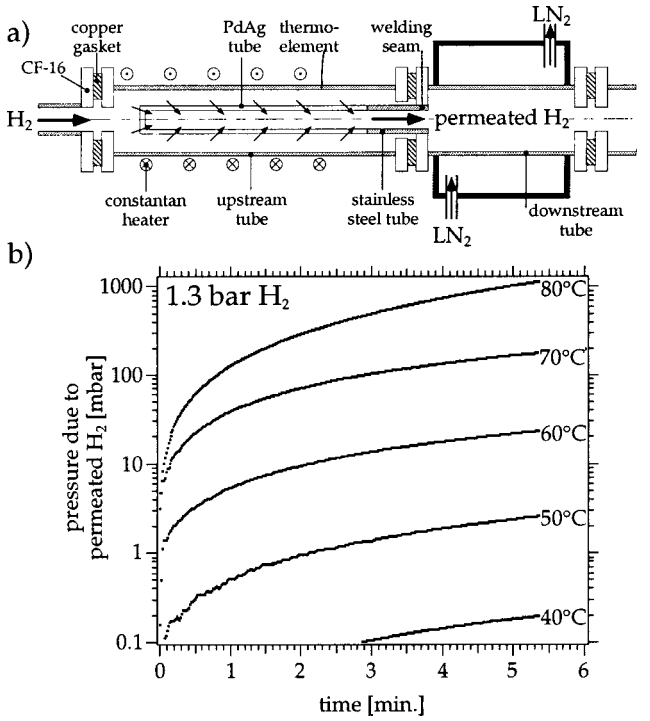

FIG. 2. (a) Detailed structure of our homemade hydrogen permeation cell which is based on a Pd–24%Ag tube. The small arrows illustrate the hydrogen permeation through the Pd–24%Ag tube. In order to improve permeation kinetics the Pd–24%Ag tube can be heated from the upstream side using the H_2 gas as heat conductor. (b) Evolution of the permeated H_2 pressure in the CF-16 cross [valves (1) and (3) closed, valve (2) open, see Fig. 1] at different temperatures of the upstream tube and for a constant H_2 upstream pressure of 1.3 bar.

The hydrogen permeability through a Pd alloy membrane can be decreased by poisoning, i.e., by the adsorption of species such as O_2 or CO on the surface. In order to get full performance of the hydrogen filter it must be activated prior to use. Slight heating to 100 °C in good vacuum or in hydrogen cleans up the surface sufficiently to provide predictable kinetics. Thus, in UHV applications the tube is simply activated during bakeout.

In order to test the integrity of our hydrogen permeation cell we applied atmospheric pressures of several gases (O_2, He, and air) at the upstream side of the activated Pd–24%Ag tube [valves (1), (2), and HPRC open, valve (3) closed (see Fig. 1)]. We found that neither the absolute pressure nor the specific partial pressures—measured with a mass spectrometer—did increase in the main UHV vessel. When applying 1.3 bar H_2 at RT, however, the pressure in the main UHV vessel (with TMP running) slowly increased reaching a constant pressure of $\approx 5\times 10^{-6}$ mbar after 30 min. After closing valve (1) the pressure in the cross was monitored with the MKS capacitance manometer. However, after more than 20 min the pressure in the cross was still below 0.1 mbar, i.e., below the resolution of the manometer. Obviously, at the selected conditions the hydrogen permeation rate through the Pd–24%Ag tube is too small to fulfill our requirements.

The downstream pressure always tends to equilibrate with the upstream pressure. The degree and rate at which this

equilibration occurs can be controlled by the temperature of the tube and the upstream pressure. However, due to the thin wall of the tube the amount of external pressure it will take without collapsing is limited. Figure 2(b) illustrates the improvement of the permeation kinetics upon application of heat. These curves are helpful for the fine tuning of the desired pressure used in the experiments. Note that in our setup the Pd–24%Ag tube is heated indirectly, i.e., hydrogen gas is used to transfer the heat from the upstream tube to the Pd–24%Ag tube. However, the downstream tube is heated by the upstream tube via the Cu gasket. Therefore, to prevent outgasing, the downstream tube is LN_2 cooled during operation.

The purity of the permeated H_2 was monitored by means of a mass spectrometer. When comparing the mass spectrum obtained from the residual gas in the UHV vessel just before H_2 dosing, with the spectra obtained during dosing unfiltered 6N-H_2 (via the bypass and without getter alloy) one sees that not only the H_2 peak intensity, but also the intensities of O_2, CO, and H_2O increased slightly. To our satisfaction, the O_2, CO, and H_2 intensities remained unchanged when the same amount of permeated H_2 was applied to the UHV vessel. However, here we want to point out that the ultimate test to check the purity of the permeated H_2 is our experiment, where we expose up to 1.3 bar H_2 to very reactive Y films (see Sec. IV).

C. Operation of the hydrogenation system

The first step to operate our hydrogenation system, thus, is to activate the different LN_2 traps (the cooling of the downstream tube is crucial for the gas purity) as well as to heat the upstream tube to the desired temperature [see Figs. 1 and 2(b)]. As soon as valves (1) and (3) are closed, one can apply the desired upstream H_2 pressure, typically 1.3 bar, to the permeation cell. The hydrogen gasflow yielding optimal purity of the gas is as follows:

It starts at the 6N-H_2 bottle, with the hydrogen gas crossing successively two LN_2 cold traps and the hydrogen permeation cell to reach finally the CF-16 cross (Fig. 1). While the pressure in the cross increases (see Fig. 2) the sample with a freshly deposited Y film is transferred into the HPRC. As soon as the desired pressure is reached, both, valve (2) as well as the HPRC have to be closed. Now the sample can be exposed to the filtered H_2 by opening valve (1). After the desired hydrogenation time the HPRC is simply evacuated by opening valve (3). Indeed the getter alloy sorbs the H_2 so efficiently that the pressure in the main UHV vessel only rises up to 5×10^{-9} mbar upon opening of the HPRC. Note, our setup is such that during the whole hydrogenation procedure the sample never is in contact with non-UHV compartments.

Figure 3 shows a typical example of the hydrogen pressure evolution (solid line) during hydrogenation of a Y dihydride film. The Y trihydride film resulting from this treatment will be discussed in Figs. 4(c), 6(c), 8(c), and 10(c). The temperature of the getter alloy (dotted line) is also shown. With the knowledge of the thickness of the Y dihydride film and the gas expansion into the HPRC when opening valve (1), the first pressure drop from 980 to about 630 mbar can be used to calculate the amount of hydrogen absorbed by the Y film. However, the film thickness calibration is rather inaccurate making a reliable volumetric concentration determination difficult. In the example shown in Fig. 3 valve (2) was reopened in order to achieve a hydrogen pressure of 1 bar. The second very sharp pressure drop illustrates the efficient pumping of the getter alloy upon opening valve (3). Moreover, the exothermic nature of the hydride formation in the getter alloy is reflected by its abrupt temperature increase up to ≈170 °C.

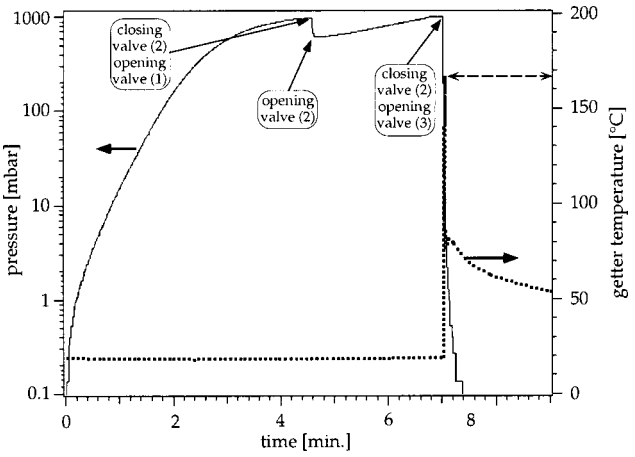

FIG. 3. Typical example of the pressure evolution (solid line) during hydrogenation of a Y dihydride film. The Y trihydride film resulting from this treatment will be discussed in Figs. 4(c), 6(c), 8(c), and 10(c). The temperature of the getter alloy (dotted line) is also shown.

IV. EXPERIMENTAL RESULTS AND DISCUSSION

A. Structural characterization: XPD and LEED results

Figures 4(a)–4(c) display the sequence of experiments starting with a Y film deposited at 700 K without any H_2 background pressure [Fig. 4(a)], a Y film deposited at 500 K under a H_2 partial pressure of 5×10^{-6} mbar [Fig. 4(b)], and the Y film of Fig. 4(b) being loaded with 1 bar purified H_2 in the HPRC during 144 [Fig. 4(c)]. XPD from the Y film deposited without any H_2 background pressure [Fig. 4(a)] reveals sixfold symmetry with a flower-like design in the center and prominent maxima at $\Theta\approx34°$ (label *U*), $\Theta\approx52°$ (label *V*), $\Theta\approx34°$ (label *W*), and $\Theta\approx50°$ (label *X*). A SSC calculation including Y atoms in eight layers of a hcp(0001) oriented cluster [Fig. 4(d)] fits nicely with the experimental diffractogram [Fig. 4(a)]. Though still sixfold symmetric, Y deposition under a H_2 partial pressure of 5×10^{-6} mbar induces drastic changes in the Y $3d_{5/2}$ diffractogram [Fig. 4(b)]. The flower-like design in the center of the diffractogram becomes wheel-like. Moreover, only maxima at $\Theta\approx34°$ (label *U*) and $\Theta\approx56°$ (label *V*) remain. The experiment is very well reproduced by a SSC calculation using eight layers of two equally populated fcc(111) domains rotated by 180° with respect to each other [Fig. 4(e)]. The fcc structure reveals the β-phase.[1] Unloading towards the α-phase [Fig. 4(a)] is achieved by heating the dihydride film

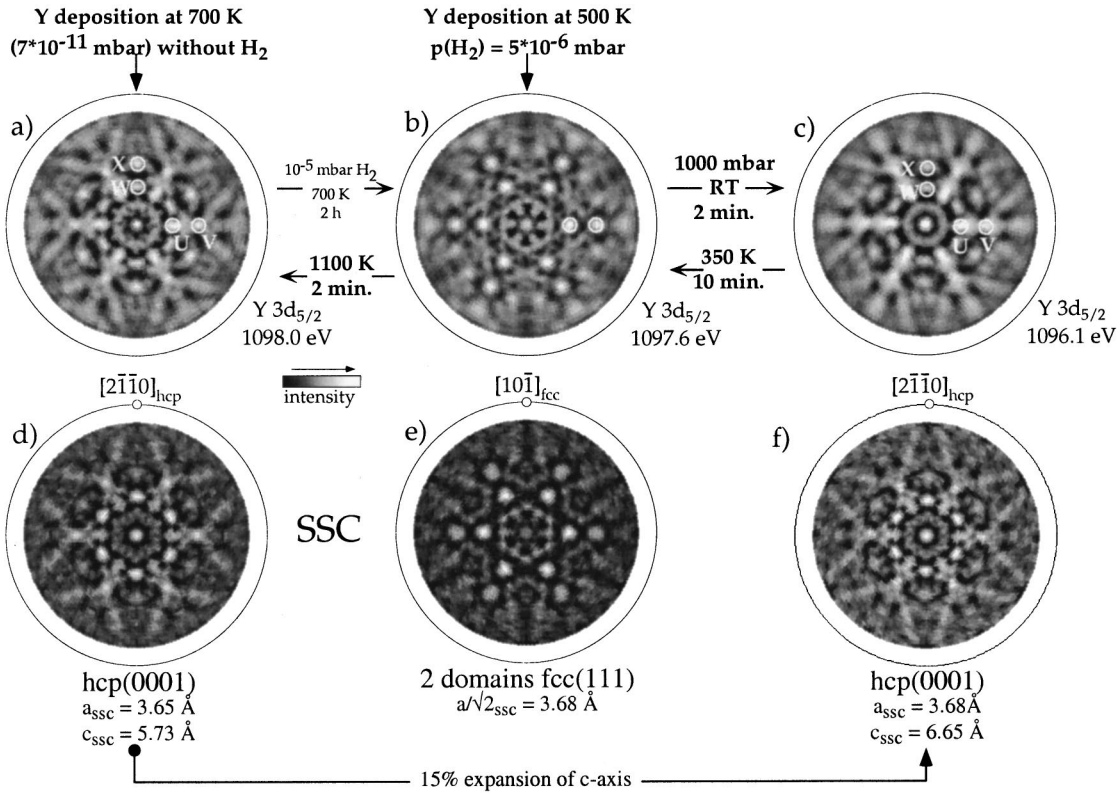

FIG. 4. Stereographic projections of experimental and calculated (SSC) Y $3d_{5/2}$ intensities. All patterns are oriented with the $[001]_{bcc}$ direction of the underlying W(110) crystal pointing to the top. Labels are explained in the text. The lattice constants used for the SSC calculations are indicated below the respective figure. (a) Y film deposited at 700 K without H_2 background pressure. (b) Y film deposited under a H_2 partial pressure of 5×10^{-6} mbar at 500 K. (c) Y film from (b) after exposure to 1 bar purified H_2 in the HPRC during 144 s. (d) Calculation including Y atoms in eight layers of an (0001) oriented hcp cluster. (e) Calculation including Y atoms in eight layers of two equally populated fcc(111) clusters rotated by 180° with respect to each other. (f) Calculation including Y atoms in eight layers of an (0001) oriented hcp cluster. Compared to the cluster used for the pattern of (d) the *c*-axis of the cluster used for (f) is expanded by 15%.

to 1100 K during 2 min. Note, that fcc(111) oriented Y dihydride films can also be produced by exposing α-phase Y films to a H_2 partial pressure of 10^{-5} mbar (700 K during 2 h).[18] Exposure of Y dihydride films to a H_2 pressure of 1 bar during 144 s (see Fig. 3) again induces drastic changes in the Y $3d_{5/2}$ diffractogram [Fig. 4(c)]. At the first view this XPD pattern is very similar to Y $3d_{5/2}$ diffractograms from hcp(0001) oriented α-phase yttrium [Figs. 4(a)]. In particular, the maxima *U*, *V*, *W*, *X* reappear. However, a closer look reveals that compared to the α-phase XPD pattern [Fig. 4(a)] these prominent maxima (labels *U*, *V*, *W*, *X*) are shifted towards the normal by ≈3°. In the case of hcp(0001) oriented crystal structures, a shift of prominent maxima towards the normal indicates an increased c/a-ratio. Assuming the basal plane lattice parameter to remain almost unchanged upon H loading (this assumption is justified by the LEED analysis below), a shift of the prominent maxima towards the normal by ≈3° corresponds to a *c*-axis expansion of ≈15%. Indeed, a SSC calculation including Y atoms in eight layers of a hcp(0001) oriented cluster where the *c*-axis is expanded by 15% compared to the α-phase *c*-axis [Fig. 4(f)] fits nicely with the experimental diffractogram [Fig. 4(c)]. In agreement with previous experiments using powder samples,[3] recent x-ray diffraction (XRD)[15] and neutron scattering[16] experiments demonstrated that thin Y trihydride films exhibit the HoD_3 structure, i.e., a structure with the Y atoms on hcp sites and the H atoms occupying unusual interstitial sites. Moreover, it was observed that the transition from α via β to γ affects mainly the *c*-axis: while the *c*-axis expands by about 15%, the change of the basal plane lattice parameter is only about 0.5%.[3] Epitaxially grown *c*-axis Y films were reported to behave similarly.[16] Thus, after exposure of a Y dihydride film to 1 bar H_2 the observation of the hcp crystal structure together with a *c*-axis expansion of ≈15% compared to the α-phase *c*-axis reveal the γ-phase. Reversibility towards the β-phase is achieved by slightly annealing the trihydride film to ≈350 K.

It is the change in the stacking sequence between the hcp (*ABAB*…) and the fcc (*ABCABC*…) phase that accounts for the disappearance of maxima caused by scattering events within next-nearest neighboring planes (labels *W*, *X*) when going from hcp [Figs. 4(a) and 4(c)] to fcc [Fig. 4(b)]. The formation of two equally populated fcc(111) domains is induced at the W(110)–Y interface. Due to the quasihexagonality of the body-centered-cubic bcc(110) surface, closed-packed Y layers can start stacking either in the *A* or *B* orientation (Fig. 5). For the fcc case this results in two (111) oriented domains rotated by 180° with respect to each other,

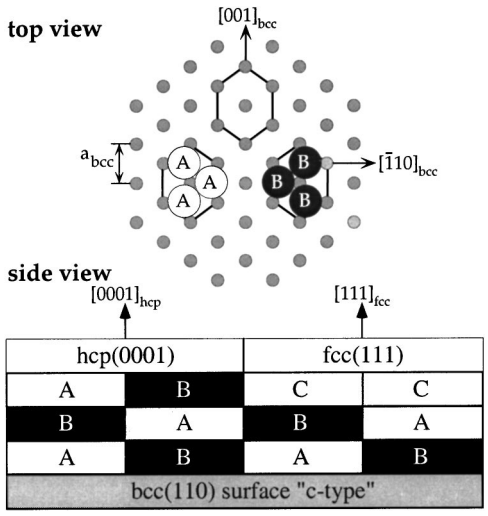

FIG. 5. Schematic drawing to illustrate the formation of two equally populated fcc(111) or two equally populated hcp(0001) domains at the W(110)–Y interface. Top view: The two possibilities (*A*,*B*) for closed-packed metal layers to start the stacking sequence on a quasihexagonal bcc(110) surface. Side view: Four different stacking sequences of close packed metal planes on bcc(110) surfaces ending up either with two (0001) oriented hcp or two (111) oriented fcc domains.

namely '*c*'*ABCABC*… or '*c*'*BACBAC*…. Here '*c*' denotes the quasihexagonal surface layer of a bcc(110) crystal. Similar for the hcp case were '*c*'*ABAB*… or '*c*'*BABA*… stacking occurs. However, if the surface is of the hcp(0001) type, then there are, due to the presence of steps on a real surface, two possible surface terminations for each domain. In the hcp(0001) case it is therefore not possible to distinguish between situations with one or two domains with XPD or LEED (see later). Finally, our XPD results show that all Y hydride films, i.e., from the α up to the γ-phase, follow the so-called Nishiama–Wassermann orientation on W(110),[43] where most densely packed metal rows ($[101]_{fcc}$,$[2\bar{1}\bar{1}0]_{hcp}$) are parallel to the $[001]_{bcc}$ axis of the bcc(110) substrate. There is a 13:15 match (within ≈1%), i.e., a supercell commensuration between the Y$[2\bar{1}\bar{1}0]_{hcp}$ distance of 3.65 Å and the W$[001]_{bcc}$ distance of 3.16 Å.

Figures 6(a)–6(c) display the sequence of LEED experiments starting with a Y film deposited at 700 K without any H_2 background pressure (α-phase) [Fig. 6(a)], a Y film deposited at 500 K under a H_2 partial pressure of 5×10^{-6} mbar (β-phase) [Fig. 6(b)], and the Y film of Fig. 6(b) being loaded with 1 bar purified H_2 in the HPRC during 144 s (γ-phase) [Fig. 6(c)]. As expected for a hcp(0001) oriented Y film, LEED from the α-phase yields a hexagonal pattern [Fig. 6(a)]. A hexagonal pattern with six equally intense spots is also observed for the β-phase [Fig. 4(b)]. It is consistent with two equally populated fcc(111) domains rotated by 180° with respect to each other. A careful analysis of the surface reciprocal lattice indicates that the surface lattice constant slightly increases (≈1%) when going from α [Fig. 6(a)] to β [Fig. 6(b)]. In turn, for the transition from β [Fig. 6(b)] to γ [Fig. 6(c)] a further increase of the basal plane lattice parameter could not be resolved with LEED. Compared to the β-phase, the observation of a (1×1) surface symmetry appears to be contradictory to neutron scattering experiments revealing the HoD_3 structure for the γ-phase.[3] Indeed, accounting for the HoD_3 structure one would, compared to the surface symmetry of the β-phase, expect a $(\sqrt{3}\times\sqrt{3})R30°$ surface symmetry for *c*-axis oriented Y trihydride films.[3,5] However, one has to remember, that the high mobility of the proton ends up with a very small Debye–Waller factor and hydrogen is not expected to contribute to the LEED pattern. Based on the LEED experiment alone we therefore can not conclude if, in the near surface region, the H atoms still occupy the peculiar interstitial sites of the HoD_3 structure, or if the wave-like H displacements, which are at the origin of the HoD_3 structure, are modified or even suppressed. In turn, the six equally intense spots observed in the γ-phase [Fig. 6(c)] are consistent with a hcp(0001) oriented Y lattice.

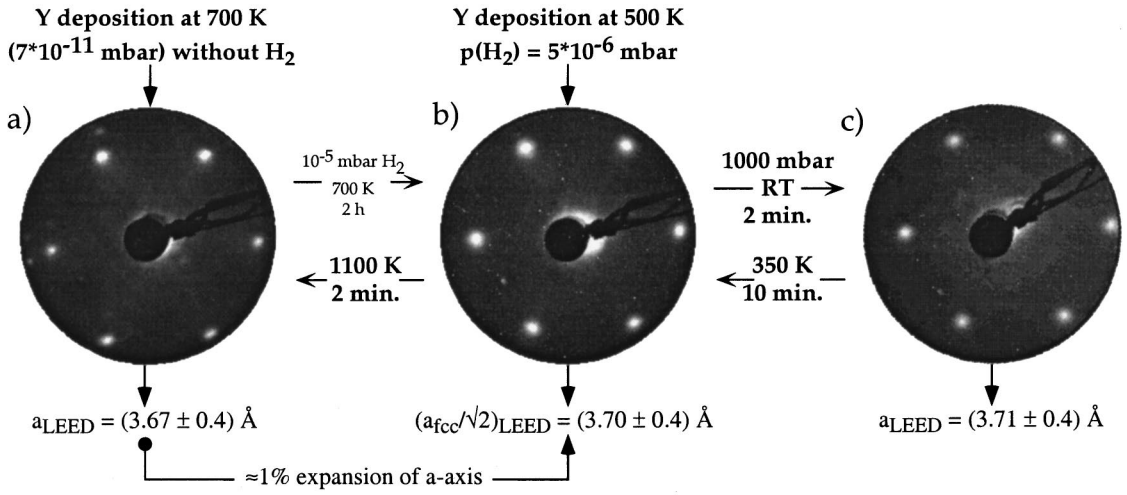

FIG. 6. LEED patterns (40 eV) taken from different Y hydride phases. Note that LEED and XPD patterns are not oriented identically. (a) Y film deposited at 700 K without H_2 background pressure (α-phase). (b) Y film deposited under a H_2 partial pressure of 5×10^{-6} mbar at 500 K (β-phase). (c) Y film from (b) after exposure to 1 bar purified H_2 in the HPRC during 144 s (γ-phase).

Except for the slight H-induced expansion of the Y lattice the lateral arrangement of Y atoms on the fcc(111) surface is the same as that on hcp(0001) surfaces. Therefore, a simple kinematic LEED pattern analysis does not provide conclusive information on the H-induced phase-transformations in yttrium. However, the high definition of the LEED spots in the different Y hydride phases [Figs. 6(a)–6(c)] is indicative for the retention of long-range order. Maintenance and identification of the short-range order is demonstrated by the well-defined XPD patterns [Figs. 4(a)–4(c)]. Therefore and despite the *c*-axis expansion of ≈15% when going from α to γ, no loss of crystallinity occurred during these H-induced structural transformations. Moreover, both of these factors are consistent with the diffusionless translation of close-packed Y planes, which is the mechanism behind *martensitic* transitions.[44]

The pure α-phase is a solid solution where the hydrogen atoms are distributed statistically in the tetrahedral interstices of the hcp Y lattice. As soon as the α-phase is saturated ($x \approx 0.2$),[1] with increasing H concentration, the system crosses the ($\alpha+\beta$) two-phase regime until the saturated α-phase has been completely converted to the pure β-phase. The equilibrium pressure at the isothermal plateau of Y dihydride is very low (10^{-6} mbar at 800 K),[1] however, further hydrogen adsorption needs much higher pressures than used in our experiments. Therefore, the H concentration of the dihydride film grown under a H_2 partial pressure of 5×10^{-6} mbar (β-phase) [Figs. 4(b) and 6(b)] corresponds to the lower boundary of the pure β-phase ($x \approx 1.99$),[1] that is a single phase dihydride with 0.01% tetrahedral vacancies. The pure β-phase also has a relatively large existence region ($\approx 1.99 \leqslant x \leqslant 2.1$)[1] and can be considered as a solid solution with the excess H atoms distributed statistically in the octahedral interstices of the fcc Y lattice (note, that octahedral occupancy occurs before all tetrahedral sites are occupied). Once the β-phase is saturated ($x \approx 2.1$), the system crosses the ($\beta+\gamma$) two-phase regime until the saturated β-phase has been completely converted to the pure γ-phase ($\approx 2.9 \leqslant x \leqslant 3.0$).[1] Due to the very slow desorption kinetics (see later) we conclude that the H concentration of the trihydride film discussed in this study [Figs. 4(c) and 6(c)] corresponds to the lower boundary of the pure γ-phase ($x \approx 2.9$),[1] that is a single phase trihydride with 0.1% octahedral vacancies.

In the following we discuss the case of Y hydride films either in the ($\alpha+\beta$) or in the ($\beta+\gamma$) two-phase regimes. This is done by means of azimuthal scans across the relevant forward focusing maxima (labels *U*, *W* in Fig. 4) and XPS core level shift and line shape analysis (see subsection IV B).

Figure 7 displays azimuthal cuts through the maxima labeled *U* and *W* (Fig. 4). While the plus signs result from a cut through Fig. 4(a) (pure α-phase), the black dots and the times signs display the equivalent azimuthal scans through a single phase Y dihydride film [Fig. 4(b)] and a single phase Y trihydride film [Fig. 4(c)], respectively. The curves with the open circles and open diamonds (their XPD pattern are not shown) were obtained after annealing a single phase Y dihydride film to 900 K during ≈2 and ≈7 min, respectively.

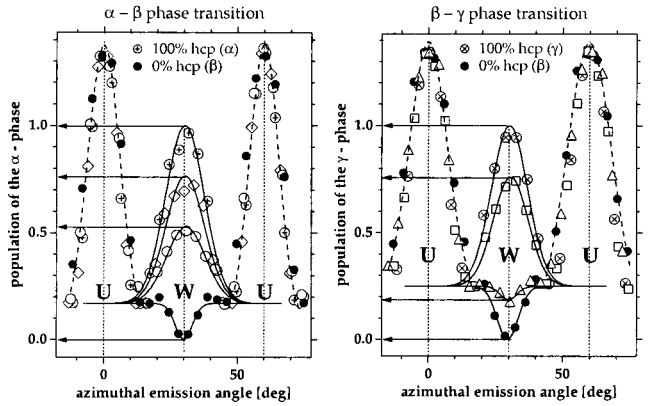

FIG. 7. Azimuthal scans illustrating the H-induced α to β (polar angle $\Theta=34°$) and β to γ (polar angle $\Theta=32°$) phase transitions. (⊕) pure α-phase film. (●) pure β-phase film. (⊗) pure γ-phase film. Y hydride films in the ($\alpha+\beta$) two-phase regime obtained upon heating a single phase Y dihydride film to 900 K during (○)≈2 min and (◇)≈7 min, respectively. Y hydride films in the ($\beta+\gamma$) two-phase regime obtained after exposing a single phase Y dihydride film during 4 min to (△) 100 mbar and (□) 200 mbar purified H_2, respectively. The hairline curves serve as a guide to the eyes to outline the *U* maxima. The solid lines are the best fits to the *W* maxima using a Gaussian function.

They are characteristic for Y hydride films in the ($\alpha+\beta$) two-phase regime. In turn, exposing a Y dihydride film to purified H_2 the transition from β to γ can be induced. Indeed, the open triangles (100 mbar during 4 min) and the open squares (200 mbar during 4 min) are characteristic for Y hydride films in the ($\beta+\gamma$) two-phase regime.

In order to obtain a straightforward estimation of the phase populations in the ($\alpha+\beta$) two-phase regime each azimuthal cut was treated as follows. First the *U* maxima were normalized between 0 and 1 for each azimuthal cut.[45] Then the respective *W* maxima were fitted with a Gaussian function (with the offset hold at zero). The solid curves in Fig. 7 are the best fits to the different cuts. Finally, each cut from films in the ($\alpha+\beta$) two-phase regime was renormalized such that the apex of the best fit to the black dots (pure β-phase, i.e., 0% hcp) equals 0 and the apex of the best fit to the plus signs (pure α-phase, i.e., 100% hcp) equals 1. For the β to γ-phase transition the same data treatment is applicable. For the ($\alpha+\beta$) two-phase regime we find that 52% (open circles in Fig. 7) and 76% (open diamonds in Fig. 7) of the Y atoms populate the α-phase. Thus, upon annealing a Y dihydride film (black dots in Fig. 7), the intensity of the *W* maxima increases as a function of decreasing H concentration. In turn, for the transition from β to γ we find that 19% (open triangles in Fig. 7) and 76% (open squares in Fig. 7) of the Y atoms populate the γ-phase, i.e., the intensity of the *W* maxima increases with increasing H concentration.

B. H concentration estimation: Y 3*d* core level analysis

Figure 8 shows the photoemission intensity in the region of the XPS Y 3*d* doublet as a function of the electron binding energy. Compared to the spectrum taken from the ''clean metal''[20] (α-phase) [Fig. 8(a)], for Y deposition under a H_2

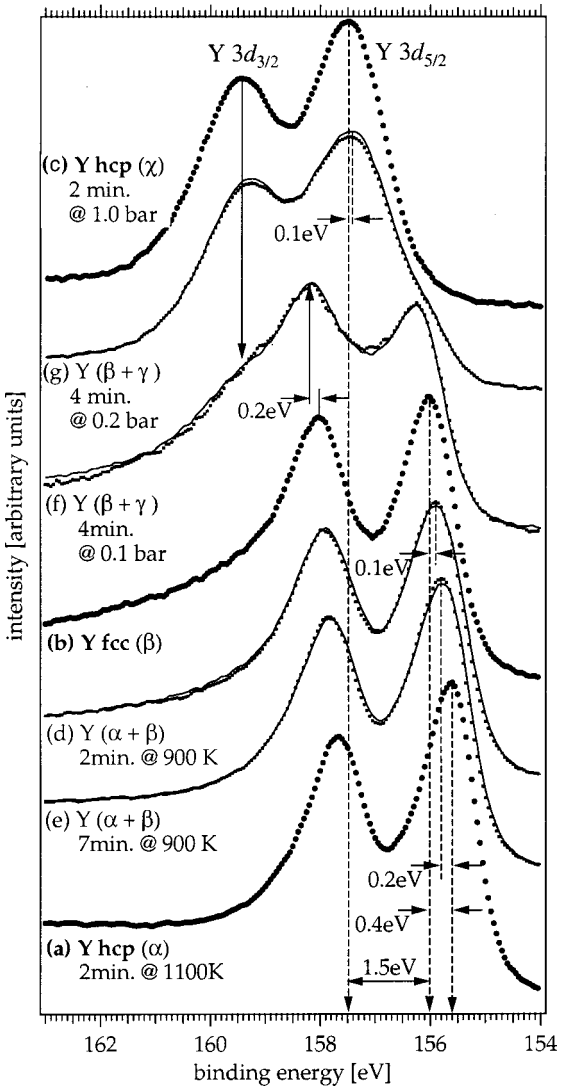

FIG. 8. XPS spectra (dots) illustrating peak positions and line shape of the Y 3*d* doublet during the H-induced phase-transitions. (a) ''clean metal''[20] film (Y deposition at 700 K without H_2 background pressure). (b) Y film deposited under a H_2 partial pressure of 5×10^{-6} mbar at 500 K (β-phase). (c) Y film from (b) after exposure to 1 bar purified H_2 in the HPRC during 144 s (γ-phase). Y hydride films in the ($\alpha+\beta$) two-phase regime obtained upon heating a single phase Y dihydride film to 900 K during (d)≈2 min and (e)≈7 min, respectively. Y hydride films in the ($\beta+\gamma$) two-phase regime obtained after exposing a single phase Y dihydride film during 4 min to (f) 100 mbar and (g) 200 mbar purified H_2, respectively. The solid curves are the best fit to the spectra (d)–(g).

partial pressure of 5×10^{-6} mbar the Y 3*d* doublet is shifted by 0.4 eV towards higher binding energies [Fig. 8(b)]. Moreover, due to an intense high-binding-energy tail the linewidth is much larger. After exposure to 1000 mbar during 144 s the Y 3*d* doublet is further shifted towards higher binding energies by 1.5 eV and its line shape is nearly symmetric [Fig. 8(c)]. Compared to the spectrum taken from the hydrogen free Y film a shift of 0.4 and 1.9 eV is comparable to values taken from polycrystalline Y dihydride and Y trihydride bulk samples, respectively.[12,13] Therefore, our interpretation of Figs. 4(b) and 4(c) in terms of single-crystalline Y dihydride and Y trihydride films is confirmed. The change in chemical environment is necessarily due to hydride formation, since in all experiments no O contamination could be detected with XPS. Moreover, for Y_2O_3 films we measure a shift of 2.5 eV.[46]

Upon annealing an Y dihydride film to 900 K the binding energy as well as the linewidth of the Y 3*d* doublet gradually decrease [Figs. 8(d) and 8(e)]. A spectrum identical to that from the ''clean metal''[20] [Fig. 8(a)] is achieved within 2 min when the dihydride film is heated to 1100 K. Exposing a Y dihydride film to 100 mbar H_2 during 4 min induces more drastic changes. The Y 3*d* doublet shifts to higher binding energies, its linewidth broadens, and, most strikingly, the Y $3d_{3/2}$ component becomes more intense than the Y $3d_{5/2}$ component [Fig. 8(f)]. Moreover, the high-binding-energy tail of the corresponding Y 3*d* doublet contains a weak shoulder whose energy position coincide with the Y $3d_{3/2}$ component of the Y trihydride spectrum [Fig. 8(c)]. Exposure to 0.2 bar H_2 further shifts the Y 3*d* doublet by 1.4 eV and, now, a weak shoulder becomes visible in the low-binding-energy tail [Fig. 8(g)].

Since XPD very directly allows for a simple linear combination of the hcp and fcc structures (see Fig. 7) the question arises whether this is also the case for the core-level spectra (Fig. 8). For the ($\alpha+\beta$) two-phase regime it turns out that a simple linear combination of (a) and (b) does fit neither (d) nor (e). Just so for the ($\beta+\gamma$) two-phase regime, i.e., a simple linear combination of (b) and (c) does not fit (f) or (g). Neither the widths nor the intensity ratios of the spin orbit split Y 3*d* are reproduced. The situation is more subtle. Very good coincidence in peak positions and intensity ratio is only achieved when the ''clean metal''[20] (dihydride) spectrum used for the linear combination is first shifted towards higher binding energies and then linearly combined with the dihydride (trihydride) spectrum. Figure 9 displays the minimal chi square of the difference between the corresponding linear combinations and the experimental spectra as a function of the shift of the ''clean metal''[20] ΔE_α (dihydride ΔE_β) spectrum towards higher binding energies. The best fits (solid lines in Fig. 8) are achieved for $\Delta E_\alpha^{\mathrm{sat}}=0.08$ eV and $\Delta E_\beta^{\mathrm{sat}}=0.19$ eV. After annealing a dihydride film to 900 K during 2 min [Fig. 8(d)] and 7 min [Fig. 8(e)] our data analysis yields an α-phase population of 49% and 73%, respectively. For the transition from β to γ we find that 26% [Fig. 8(f)] and 80% [Fig. 8(g)] of the Y atoms populate the γ-phase. Thus, the phase populations determined with our core level analysis procedure is in good agreement with the XPD results (see Fig. 7 and Table I).

Our core level analysis procedure can be explained within the following model. As the H concentration increases in the α-phase the line shape of the Y 3*d* doublet is not modified. Due to charge transfer from Y to H, however, its peak position shifts towards higher binding energy. Within the α-phase ($x\leqslant0.2$) the concentration is therefore estimated via the chemical shift of the Y 3*d* doublet. Thus, referring to the ''clean metal''[20] spectrum the quantity $\Delta E_\alpha^{\mathrm{sat}}$ corresponds to the shift of the saturated α-phase spectrum. In the ($\alpha+\beta$) two-phase regime spectra can be reproduced by a linear com-

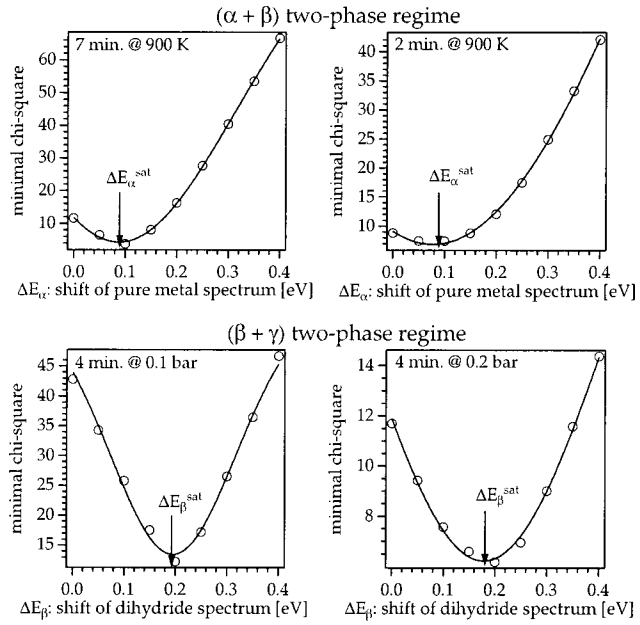

FIG. 9. Minimal chi square of the difference between the experimental spectra [Figs. 8(d)–8(g)] and spectra obtained by linearly combining the ''clean metal''[20] (dihydride) and the dihydride (trihydride) spectra as a function of the shift of the ''clean metal''[20] ΔE_α (dihydride ΔE_β) spectrum towards higher binding energies. The best fits (solid lines in Fig. 8) are achieved for $\Delta E_\alpha^{\mathrm{sat}}=0.08$ eV and $\Delta E_\beta^{\mathrm{sat}}=0.19$ eV. Note, that according to our model $\Delta E_\alpha^{\mathrm{sat}}$ and $\Delta E_\beta^{\mathrm{sat}}$ correspond to the shift of the saturated α-phase spectrum compared to the ''clean metal''[20] spectrum and to the shift of the saturated β-phase spectrum compared to the spectrum from the lower boundary of the pure dihydride.

bination of the spectrum from the saturated pure α-phase with the one obtained from the Y film at the lower boundary of the pure β-phase ($x\approx1.99$) [Fig. 8(b)]. It is analogous for the β to γ transition. In the pure β-phase ($\approx1.99\leqslant x\leqslant2.1$) the line shape of the spectrum from the Y film at the lower boundary of the pure β-phase is not modified, but with increasing x it shifts towards higher binding energies by $\Delta E_\beta^{\mathrm{sat}}$. In the ($\beta+\gamma$) two-phase regime spectra can be reproduced by a linear combination of the spectrum from the saturated pure β-phase with the one obtained from the Y film at the lower boundary of the pure γ-phase ($x\approx2.9$) [Fig. 8(c)]. From the resulting phase population coefficients the H concentration can be calculated easily (see Table I).

Our spectroscopic H estimation method is supported by the fact that the Y $3d$ spectrum taken from a $YH_{2.3}$ film [see Fig. 8(f)] is almost identical to spectra taken from polycrystalline $YH_{2.1}$ bulk samples (see Fig. 1 in Ref. 12). Note that the composition of the polycrystalline $YH_{2.1}$ bulk samples was determined gravimetrically.[12] In general, this model allows to evaluate H concentrations up to the lower boundary of the pure γ-phase ($x\approx2.9$) by means of photoelectron spectra of the Y $3d$ doublet. Since already low O contaminations induce substantial changes in the shape and energy position of the Y $3d$ doublet,[46] this method requires very clean samples. Moreover, estimated concentrations are based on the literature values of the critical H concentration for the saturated α-phase ($x\approx0.2$), for the lower boundary of the pure β-phase ($x\approx1.99$), for the saturated β-phase ($x\approx2.1$), and for the lower boundary of the pure γ-phase ($x\approx2.9$). Unfortunately these values are rather widely scattered depending on the material purity.[1] Therefore, the uncertainty of our H concentration estimation is about ±0.1. However, this spectroscopic *in situ* method is very promising in that in may also be applied to H-induced transitions in other RE hydrides.

The trihydride film discussed in this study [Figs. 4(c), 6(c), and 8(c)] was prepared by exposing a dihydride film in the HPRC to 1000 mbar purified H_2 during 144 s (see Fig. 3). At RT the equilibrium pressure of the isothermal plateau of Y trihydride is $\approx1\times10^{-3}$ mbar.[1] After the desired hydrogenation time the HPRC is evacuated from hydrogen and the sample is transfered back to the main UHV vessel (base pressure in the lower 10^{-11} mbar regime). It is, therefore, surprising that the film remains in the pure trihydride phase during several hours. Obviously molecular H_2 desorbs very slowly from clean Y (tri)hydride films. In general, the overall kinetics of hydrogen desorption is determined by the slowest of the series of steps: nucleation and growth of the metal or different hydride phases, diffusion of atomic hydrogen (across the metal or hydride phase), transition from bulk sites via subsurface sites to the surface, surface migration of chemisorbed atomic H, the recombination of two H atoms diffusing on the surface to a H_2 molecule to regain the heat of dissociation in order to overcome the heat of chemisorption, and, finally, the transport of molecular hydrogen away from the surface. As explained in the following we presume

TABLE I. Phase populations and estimated H concentrations x for different Y hydride films in the two-phase regimes. For each film the results obtained from XPD and XPS core level analysis are indicated.

	Y dihydride film ($x\approx1.99$)							
	Annealed to 900 K during				Exposed during 4 min to			
	7 min		2 min		100 mbar H_2		200 mbar H_2	
Population	XPD	XPS	XPD	XPS	XPD	XPS	XPD	XPS
% α-phase	76	73	52	49	⋯	⋯	⋯	⋯
% β-phase	24	27	48	51	81	74	24	20
% γ-phase	⋯	⋯	⋯	⋯	19	26	76	80
Estimated x	0.63	0.68	1.06	1.11	2.25	2.31	2.71	2.74

that the transition from subsurface sites to the surface is the rate-limiting process.

On the one hand, it is well known that upon H adsorption the distance between close-packed Y layers increases (by $\approx$15% when going from α to γ).[1,3] On the other hand I-V LEED data demonstrate that the interatomic distances between the first few surface layers of hcp(0001) oriented heavy RE crystals relax.[47,48] Since Y and the heavy RE are very similar from a chemical point of view and have, modulo the lattice constants, identical surface terminations, similar relaxations can be expected at the Y(0001) surface. Since relaxation in the top metal layer is energetically favorable as compared to deeper layers, subsurface H sites are expected to become more stable than bulk sites. Taking account of the exothermic nature of Y dihydride ($\Delta H_{\alpha\rightarrow\beta} = -113$ kJ/mol) and Y trihydride ($\Delta H_{\beta\rightarrow\gamma} = -44.85$ kJ/mol) formation, we conclude that the potential energy barrier a H atom has to overcome during the transition from subsurface sites to bulk sites is smaller than that for the transition from subsurface sites to the surface. Thus, the fact that the distance between the first layers can be adjusted more easily than between planes in the bulk has two important consequences. First, it reduces the number of H atoms diffusing on the surface drastically. Consequently, the probability for two H atoms diffusing on the surface to meet each other and to recombine to a H_2 molecule is very small. Molecular H_2 therefore desorbs very slowly from Y hydride films. Second, it leads for all H concentrations to an enhanced hydrogen content in the subsurface region.

Considering a Y hydride film immediately after exposure to 1000 mbar purified H_2 during 144 s [Figs. 4(c), 6(c), and 8(c)] the H concentration, therefore, is expected to increase very sharply from zero to its maximal value ($x_{\max}\approx 2.9$) when going from the vacuum to the subsurface region. Within the film the H concentration will remain constant and then gradually decrease to zero when approaching the Y–W interface. It is obvious that due to the very slow H_2 desorption discussed above the overall H concentration of the film will reduce as a function of time. However, since the potential energy barrier for transitions from bulk sites to subsurface sites is expected to be significantly smaller than for transitions from subsurface sites to the surface, H atoms leaving the subsurface region towards the surface will be replaced with H atoms diffusing from deeper regions of the film at once. Thus, while the H concentration slowly decreases in deeper regions of the film, in the subsurface region the pure triydride phase outlives. Taking account of the surface sensitivity of the photoemission experiment[49] it is then no longer surprising that from the view point of photoemission Y trihydride films outlive during several hours.

Different studies support our scenario of an enhanced H concentration in the subsurface region. In particular, a strongly enhanced near-surface solubility was reported for Nb and Pd,[50,51] suggested for polycrystalline Y films[14] and predicted for Sc(0001).[52] In CeH_{2+y}, however, the opposite was observed: At low temperatures some surface hydrogen seems to diffuse into the bulk leading to a H-depleted CeH_2 surface.[53,54] Accounting for the thermally induced lattice contraction, this phenomenon appears to be contradictory to our scenario. However, this is not the case. Ce hydrides are particular in that for hydrogen concentrations above $x=2$ the lattice contracts upon H loading. Thus, if cooling itself starts to contract the lattice, it induces a redistribution of hydrogen atoms with an infinitesimal increase of bulk concentration and some depletion at the surface, where the expansion is energetically favorable. Nevertheless, further experiments are required to check the above scenario.

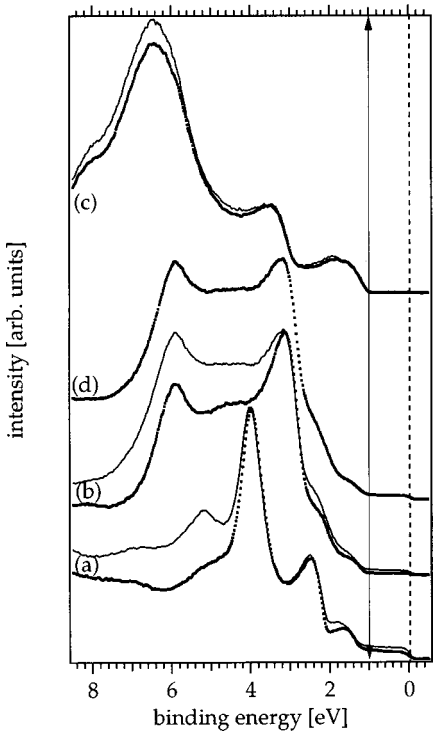

FIG. 10. Normal emission photoelectron spectra (monochromatized He I, $h\nu=21.2$ eV) illustrating the effect of contaminations on the measured spectra as well as the influence of the H_2 purity on the H uptake rate. Binding energies are referred to the Fermi level. The dotted curves and solid lines represent spectra measured, respectively, immediately and $\approx$4 h after the preparation was accomplished. (a) $YH_{1.99}$ (Y deposited under a H_2 partial pressure 5×10^{-6} mbar at 500 K). (b) $YH_{2.7}$ (clean $YH_{1.99}$ film after exposure to 200 mbar purified H_2 in the HPRC during 240 s). (c) $YH_{2.9}$ (clean $YH_{1.99}$ film after exposure to 1000 mbar purified H_2 in the HPRC during 144 s). (d) Slightly contaminated $YH_{2.7}$ (clean $YH_{1.99}$ film after exposure to 1000 mbar unfiltered 6N-H_2 in the HPRC during 180 s).

C. ARUPS results

To our knowledge the ARUPS data discussed in the following are the first ARUPS spectra from single-crystalline Y hydride films. However, since the present article deals with the preparation and characterization of clean single-crystalline YH_x films ($0\leqslant x\leqslant 2.9$) in this paragraph we focus on the effect of contaminations on the measured spectra as well as on the influence of the H_2 purity on the H uptake rate. The H-induced metal–insulator transition in Y, which is unequivocally confirmed by these spectra, will be discussed elsewhere.[21]

Figure 10 displays He I exited electron energy distribution curves obtained in normal emission as a function of the elec-

tron binding energy. To begin with, let us briefly consider the cleanest spectra [dotted curves of Fig. 10(a)–10(c)]. We find that with increasing x, i.e., when going from $YH_{1.99}$ [Fig. 10(a)] via $YH_{2.7}$ [Fig. 10(b)] to $YH_{2.9}$ [Fig. 10(c)], the electron emission shifts to higher binding energies, and the formation of hydrogen-induced bands is revealed. Moreover, the intensity at E_F gradually fades out to end up with a gap extending as far as 1 eV below E_F in the trihydride [Fig. 10(c)]. Assuming the gap to be symmetric around E_F our finding fits nicely with optical transmission spectroscopy data taken from Pd capped polycrystalline Y trihydride films revealing a gap of $\approx$1.8 eV.[2,17] Note, that valence band spectra of Y hydride films within the $(\beta+\gamma)$ two-phase regime [Fig. 10(b)] cannot be explained by linearly combining the spectra from the pure dihydride phase [Fig. 10(a)] and the pure trihydride phase [Fig. 10(c)]. Obviously, the situation is more subtle.

Naturally and as revealed by XPS, the contamination level of the Y hydride films slowly increases with time. The effect of the increasing contamination level on the measured spectra becomes evident by comparing the dotted curves (spectra measured immediately after the preparation was accomplished) with the solid lines (spectra measured $\approx$4 h after the preparation was accomplished) of Figs. 10(a)–10(c). Obviously, the increasing contamination level affects mainly states above $\approx$4 eV binding energy. Below $\approx$4 eV binding energy, however, the spectra are scarcely modified after $\approx$4 h. In particular, in the case of the trihydride [Fig. 10(c)], the gap is still present. These observations further confirm that molecular H_2 desorbs very slowly from clean Y hydride films.

All films within the $(\beta+\gamma)$ two-phase regime and the γ-phase discussed so far were prepared by exposing a clean Y dihydride film to purified H_2, i.e., to H_2 permeated through the Pd–24%Ag tube (see Sec. III). In contrast, the spectrum of Fig. 10(d) was taken after loading a clean Y dihydride film with ''unfiltered'' 6N-H_2 (1000 mbar during 180 s). The ''unfiltered'' 6N-H_2 was dosed via the bypass with the LN_2 cold traps activated as well as with the getter alloy in the getter chamber (see Fig. 1). Surprisingly, the spectra of Figs. 10(d) and 10(c) ($YH_{2.9}$ film) are completely different even though both were taken after exposing a clean Y dihydride film to 1000 mbar H_2 during 180 and 144 s, respectively. The spectrum of Fig. 10(d), however, is very similar to the spectrum of the slightly contaminated $YH_{2.7}$ film [solid line of Fig. 10(b)]. This is in agreement with the analysis of the corresponding Y $3d$ core level (not shown) yielding an x value of $\approx$2.7. Thus, after exposing a clean Y dihydride film to 1000 mbar ''unfiltered'' 6N-H_2 during 180 s the film is within the $(\beta+\gamma)$ two-phase regime, while after exposure to 1000 mbar permeated H_2 during 144 s the γ-phase is fully developed. Moreover, we conclude that H_2 permeated through the Pd–24%Ag tube is cleaner than 6N-H_2 subjected to several LN_2 cold traps. As already speculated by Kremers *et al.*,[17] our observation indicates that the H adsorption rate strongly depends on the H_2 purity. The catalytic activity of yttrium itself for hydrogen dissociation must therefore be considerable, but very sensitive to poisoning of the surface.

V. SUMMARY

In summary, we have successfully prepared and characterized clean, single-crystalline YH_x films ($0 \leqslant x \leqslant 2.9$) on a W(110) crystal. We find that direct Y dihydride ($x \approx 1.99$) growth, i.e., Y evaporation under a H_2 partial pressures of $\approx 5\times10^{-6}$ mbar at 500 K on W(110), is the most convenient starting point for the preparation of clean single-crystalline Y hydride films covering H concentrations from the clean metal ($x \approx 0$) up to the lower boundary of the pure γ-phase ($x \approx 2.9$). In contrast to the case of H loading after Y deposition,[18] directly grown Y dihydride films are free of any contamination, and their preparation is simple and well reproducible. On the one hand, it is possible to adjust the desired H concentration within the α-phase ($x \leqslant \approx 0.2$) or the $(\alpha+\beta)$ two-phase regime ($\approx 0.2 \leqslant x \leqslant \approx 1.99$) upon annealing Y dihydride films. On the other hand transferring Y dihydride films into our homemade UHV compatible HPRC and exposing them up to 1000 mbar purified H_2 the transition from β to γ ($x \geqslant \approx 2.9$) can be induced within a few minutes. Care was taken that the H loading/unloading procedure, the LEED experiment, and the sample transfer to the analysis position were done within 15 min after the Y deposition was accomplished. Most satisfactory we note, that $\approx$30 min after Y deposition the oxygen contamination level still was below the limit of detectability of XPS. However, one should keep in mind that due to the residual gas the O contamination level of both Y and Y hydride films increases by $\approx$0.2% per hour (cross section corrected O $1s$ to Y $3d$ intensity ratio), and, consequently, the measuring time for reliable photoemission experiments is limited by the requirement of clean samples to $\approx$4 h. Note, that in contrast to previous studies,[2,15–17] preparation and experiments are done *in situ*, and the films are not capped by a protective Pd layer.

We would like to point out that it is the extension of our spectrometer with the homemade UHV compatible hydrogenation system presented in Sec. III, that made it possible to load clean Y dihydride films up to the trihydride phase *in situ*. The hydrogenation system combines a HPRC with an hydrogen permeation cell based on a Pd–24%Ag tube. The hydrogen permeation cell is used to remove impurities from gaseous 6N hydrogen and, thus, to minimize the contamination of the films during H_2 exposure in the HPRC. After the desired hydrogenation time the HPRC is, for the same reason, evacuated by a simple realization of an oil-free pumping system, namely a sorption pump based on a getter alloy (70%Zr–24.6%V–5.4%Fe) absorbing hydrogen efficiently at RT. The overall design is such that the sample never gets in contact with non-UHV compartments. Our hydrogenation system is routinely used with hydrogen pressures up to 1.3 bar.

For direct Y dihydride growth on W(110) the formation of two equally populated fcc(111) domains rotated by 180° with respect to each other is observed. The formation of different domains is induced at the W(110)–Y interface. Due

to the quasihexagonality of the bcc(110) surface, close-packed Y layers start stacking either in the *A* or *B* orientation. In the α and γ-phase, were the Y atoms occupy the lattice sites of a hcp(0001) oriented crystal, we also expect the prescence of two equally populated domains rotated by 180° with respect to each other. However, if the surface is of the hcp(0001) type, neither XPD nor LEED can distinguish between situations with one or two domains. Most importantely XPD and LEED demonstrate that, despite of the *c*-axis expansion of ≈15% when going from α to γ, no loss of crystallinity occurred during the H-induced *martensitic transformations* of the Y lattice. Moreover, all Y hydride films, i.e., from the α up to the γ-phase, follow the so-called Nishiama–Wassermann orientation[43] on W($\underline{1}\underline{1}0$), where most densely packed metal rows ($[101]_{\mathrm{fcc}}$,$[2\bar{1}10]_{\mathrm{hcp}}$) are parallel to the $[001]_{\mathrm{bcc}}$ axis of the bcc(110) substrate.

Our model for H concentration estimation esthablished previously for the α to β-phase transition,[18] has been successfully extended to the β to γ-phase transition. It is based on line shape and peak position analysis of the Y 3*d* core level. Note that we can monitor peak position and line shape of the Y 3*d* during annealing the sample on the analysis position, thus, we can adjust the desired H concentration within the α-phase or the $(\alpha+\beta)$ two-phase regime easily. Consistent with the XPS analysis, XPD offers the possiblility to directly determine the phase population in the two-phase regimes.

When going from the dihydride to the trihydride normal emission ARUPS data reveal the formation of hydrogen-induced bands. Moreover, the intensity at E_F gradually fades out to end up with a gap extending as far as 1 eV below E_F in the trihydride. The slowly increasing contamination level affects mainly states above ≈4 eV binding energy, while states below ≈4 eV binding energy are scarcely modified ≈4 h after the Y deposition was accomplished. Moreover, the importance to remove impurities from gaseous 6N hydrogen using the hydrogen permeation cell becomes evident when comparing ARUPS data taken from Y hydride films after exposure to 1000 mbar 6N-H_2 during 180 s with films exposed to 1000 mbar purified H_2 during 144 s. In the case of ''unfiltered'' hydrogen a slightly contaminated film within the $(\beta+\gamma)$ two-phase regime results, while for permeated hydrogen the film is clean and the γ-phase is fully developed. Furthermore, this observation indicates that the H adsorption rate strongly depends on the H_2 purity. The catalytic activity of yttrium itself for hydrogen dissociation must therefore be considerable, but very sensitive to poisoning of the surface. Finally, the fact that the pure trihydride phase outlives during several hours when the sample is handeled under UHV conditions, demonstrates that molecular H_2 desorbs very slowly from clean Y (tri)hydride films. A scenario based on enhanced H concentration in the subsurface region combined with the surface sensitivity of the photoemission experiment is proposed to explain this from the viewpoint of thermodynamics surprising observation.

The results presented in this article demonstrate the capability of our experimental setup for *in situ* investigations on the geometrical and electronic structure of Y hydrides as a function of the H content using angle-resolved photoelectron spectroscopy. We would like to point out that the application of our setup is by no means limited to Y hydrides. Indeed, clean single-crystalline Yb hydride films have been investigated succesfully,[55] and the preparation and investigation of the other RE hydrides should be possilbe as well. In future experiments we plan to study not only the concentration dependence, but also the temperature dependence of the structures and electronic properties observed in the different phases of RE hydrides. For example the temperature induced metal–insulator transitions reported for superstoichiometric REH_{2+x} (here RE=Y, Gd, Ho, Er) between 250 and 300 K[1] warrants to be investigated with photoemission.

ACKNOWLEDGMENTS

The authors profited from stimulating discussions with R. G. Agostino and J. Osterwalder. Skillful technical assistance was provided by S. Abate, F. Bourqui, E. Mooser, Ch. Neururer, O. Raetzo, and R. Schmid. The ST707® getter pills have been generously provided by SAES Getters S.p.A., Viale Italia 77, 20020 Lainate, MI, Italy. This project has been supported by the Fonds National Suisse pour la Recherche Scientifique.

[1] P. Vajda, in *Handbook on the Physics and Chemistry of Rare Earths*, edited by K. A. Gschneider and L. Eyring (Elsevier, Amsterdam, 1995), Vol. 20.
[2] J. N. Huiberts, R. Griessen, J. H. Rector, R. J. Wijngaarden, J. P. Dekker, D. G. de Groot, and N. J. Koeman, Nature (London) **380**, 231 (1996).
[3] T. J. Udovic, Q. Huang, and J. J. Rush, J. Phys. Chem. Solids **57**, 423 (1996).
[4] J. P. Dekker, J. van Ek, A. Lodder, and J. N. Huiberts, J. Phys.: Condens. Matter **5**, 4805 (1993).
[5] Y. Wang and M. Y. Chou, Phys. Rev. Lett. **71**, 1226 (1993).
[6] R. Ahuja, B. Johansson, J. M. Wills, and O. Eriksson, Appl. Phys. Lett. **71**, 3498 (1997).
[7] P. J. Kelly, J. P. Dekker, and R. Stumpf, Phys. Rev. Lett. **78**, 1315 (1997).
[8] K. K. Ng, F. C. Zhang, V. I. Anisimov, and T. M. Rice, Phys. Rev. Lett. **78**, 1311 (1997).
[9] R. Eder, H. F. Pen, and G. A. Sawatzky, Phys. Rev. B **56**, 10115 (1997).
[10] J. H. Weaver, D. T. Peterson, and R. L. Benbow, Phys. Rev. B **20**, 5301 (1979).
[11] J. H. Weaver, D. T. Peterson, R. A. Butera, and A. Fujimori, Phys. Rev. B **32**, 3562 (1985).
[12] A. Fujimori and L. Schlapbach, J. Phys. C **17**, 341 (1984).
[13] J. Osterwalder, Z. Phys. B: Condens. Matter **61**, 113 (1985).
[14] R. Baptist, A. Pellissier, and G. Chauvet, Z. Phys. B: Condens. Matter **73**, 107 (1988).
[15] A. Remhof, G. Song, K. Theis-Bröhl, and H. Zabel, Phys. Rev. B **56**, R2897 (1997).
[16] A. Remhof, G. Song, Ch. Sutter, A. Schreyer, R. Siebrecht, H. Zabel, F. Güthoff, and J. Windgasse, Phys. Rev. B **59**, 6689 (1999).
[17] M. Kremers, N. J. Koeman, R. Griessen, P. H. L. Notten, R. Tolboom, P. J. Kelly, and P. A. Duine, Phys. Rev. B **57**, 4943 (1998).
[18] J. Hayoz, S. Sarbach, Th. Pillo, E. Boschung, D. Naumović, P. Aebi, and L. Schlapbach, Phys. Rev. B **58**, R4270 (1998).
[19] A. Remhof (private communication).
[20] The strong affinity of yttrium for hydrogen (enthalpy of solution $\Delta H_\alpha = -82$ kJ/mol) makes it impossible to prepare Y films totally free of hydrogen. Even for deposition from a LN_2 cooled evaporation cell at pressures never exceeding 7×10^{-11} mbar Y reacts with ambient H_2. In the context of the present study the notation ''clean metal'' therefore

means Y films with an oxygen contamination level below the limit of detectability of XPS, but with very small concentrations of H atoms solved in the Y lattice.
[21]J. Hayoz, Ph.D. thesis, University of Fribourg, Switzerland, 1999; J. Hayoz, M. Bovet, Th. Pillo, L. Schlapbach, and P. Aebi (unpublished).
[22]C. S. Fadley, in *Synchrotron Radiation Research: Advances in Surface Science*, edited by R. Z. Bachrach (Plenum, New York, 1990), Vol. 1.
[23]P. Aebi *et al.*, Surf. Sci. **402–404**, 614 (1998).
[24]J. Osterwalder *et al.*, Surf. Sci. **331–333**, 1002 (1995).
[25]R. Fasel, P. Aebi, R. G. Agostino, D. Naumović, J. Osterwalder, A. Santaniello, and L. Schlapbach, Phys. Rev. Lett. **76**, 4733 (1996).
[26]J. Hayoz, D. Naumović, R. Fasel, P. Aebi, and L. Schlapbach, Surf. Sci. **373**, 153 (1997).
[27]J. Hayoz, Th. Pillo, R. Fasel, L. Schlapbach, and P. Aebi, Phys. Rev. B **59**, 15975 (1999).
[28]D. Gregory and M. Fink, At. Data Nucl. Data Tables **14**, 39 (1974).
[29]Th. Pillo, L. Patthey, E. Boschung, J. Hayoz, P. Aebi, and L. Schlapbach, J. Electron Spectrosc. Relat. Phenom. **97**, 243 (1998).
[30]P. Aebi, J. Osterwalder, R. Fasel, D. Naumović, and L. Schlapbach, Surf. Sci. **307–309**, 917 (1994).
[31]Th. Pillo, J. Hayoz, H. Berger, M. Grioni, L. Schlapbach, and P. Aebi, Phys. Rev. Lett. **83**, 3494 (1999).
[32]R. G. Agostino, P. Aebi, J. Osterwalder, J. Hayoz, and L. Schlapbach, Surf. Sci. **384**, 36 (1997).
[33]Danish Micro Engineering, Herlev, Denmark.
[34]S. Sarbach, Diploma thesis, University of Fribourg, Switzerland, 1998.
[35]S. Horch, H. T. Lorensen, S. Helveg, E. Lægsgaard, I. Stensgaard, K. W. Jacobsen, J. K. Nørskov, and F. Besenbacher, Nature (London) **398**, 134 (1999).
[36]SAES Getters S.p.A., Viale Italia 77, 20020 Lainate, MI, Italy.
[37]F. Doni, C. Boffit, and B. Ferrario, J. Vac. Sci. Technol. A **46**, 2447 (1986).
[38]F. A. Lewis, *The Palladium Hydrogen System* (Academic, New York, 1967).
[39]D. Fort, J. P. G. F. Arr, and I. R. Harris, J. Less-Common Met. **39**, 293 (1975).
[40]S. Q. Zhang, A. E. Fouda, and T. Matsuura, J. Membr. Sci. **70**, 249 (1992).
[41]V. V. Latyshev and V. M. Bystritskiy, Phys. Met. Metallogr. **71**, 1 (1991).
[42]J. Shu, B. P. A. Grandjean, A. van Nest, and S. Kaliaguine, Can. J. Chem. Eng. **69**, 1036 (1991).
[43]L. A. Bruce and H. Jaegger, Philos. Mag. A **38**, 223 (1978).
[44]J. W. Christian, *The Theory of Transformation in Metals and Alloys*, 2nd ed. (Pergamon, Oxford, 1981).
[45]The number of scattering events causing the *U* maxima remains unchanged during the transition from hcp(0001) to two equally populated fcc(111) domains.
[46]J. Hayoz, Ph.D. thesis, University of Fribourg, Switzerland, 1999; J. Hayoz, M. Bovet, Th. Pillo, L. Schlapbach, and P. Aebi (submitted).
[47]S. Tougaard and A. Ignatiev, Surf. Sci. **115**, 270 (1982).
[48]S. C. Wu, H. Li, Y. S. Li, D. Tian, J. Quinn, F. Jona, and D. Fort, Phys. Rev. B **44**, 13720 (1991).
[49]For electron kinetic energies relevant in the present study, i.e., the 20–1100 eV regime, the elastic mean free path varies from 2.4 to 7.5 monolayers [M. P. Seah and W. A. Dench, Surf. Interface Anal. **1**, 2 (1979)]. Thus, in the case of Y(0001) ($c=5.73$ Å) the elastic mean free path varies from 7 to 22 Å, while for *c*-axis oriented trihydride films ($c=6.60$ Å) it varies from 8 to 25 Å.
[50]M. Strongin, J. Colbert, G. J. Dienes, and D. O. Welch, Phys. Rev. B **26**, 2715 (1982).
[51]M. A. Pick, A. Hanson, K. W. Jones, and A. N. Goland, Phys. Rev. B **26**, 2900 (1982).
[52]P. Feibelman and D. Hamann, Solid State Commun. **34**, 215 (1980).
[53]L. Schlapbach, J. P. Burger, P. Thiry, J. Bonnet, and Y. Petroff, Phys. Rev. Lett. **57**, 2219 (1988).
[54]L. Schlapbach, in *Hydrogen in Intermetallic Compounds I*, edited by L. Schlapbach (Springer, Berlin, 1992).
[55]J. Hayoz, Ph.D. thesis, University of Fribourg, Switzerland, 1999; J. Hayoz, M. Bovet, Th. Pillo, L. Schlapbach, and P. Aebi (unpublished).